INJECTION AND EJECTION SYSTEMS FOR THE GANIL SSC

J. Fermé, G. Gendreau, P. Yvon
GANIL, B.P. 1, 91406 Orsay, France

Summary

The injection and ejection systems (1) planned for the Separated Sector Cyclotrons are shortly described. The main effort was devoted to the study of the non resonant extraction mechanism (ν_x = 1.2) for high energy light ions (C^{6+} - 100 MeV/A). A separated turn ejection is provided by adding a first harmonic field bump $\Delta B(x,\theta)$ with maximum gradient 67 G/cm. The beam behavior is entirely explained from the solution of the first order perturbed radial equation of motion.

1. Introduction

A general description of the GANIL project is given in an invited paper. Fig. 1 shows schematically the beam history. Particles coming from a compact injector cyclotron C_o enter a series of two identical SSC.

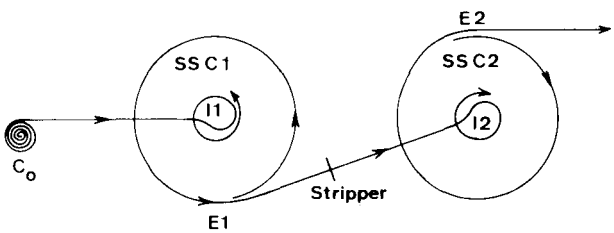

Fig. 1 General beam pattern

They cross identical injection systems I_1, I_2 and two identical ejection systems E_1, E_2. Both systems use basically the same components which are crossed in opposite ways. The main problem comes from the turn separation σ which is very different for the whole range of particles, charges and energies covered by the machine. In order to limit the range of the radial deflector position, it is more convenient to quantify σ by choosing adequate values of the RF voltage. But, for high energy light ions (C^{6+} - 100 MeV/A), σ is less than the beam width (2.5 mm ÷ 5 mm) for the maximum voltage. The turn spacing must therefore be enhanced by a beam bump.

The beam trajectories through I_i, E_i are computed with TRAJ 30 (2). The magnetic field map of the cyclotron used in the code is a synthetic one, looking like the field measured in the 1/11 scale NHL model in the stray field, isochronized in the good field region. The field drawn from recent measurements on the four sectors, .15 scale NHL model (reported in this book) will be used in the near future. Furthermore, the perturbation brought by iron C or H shaped magnetic deflectors on the main field are not considered.

2. Injection

The injection schemes are drawn on Fig. 2 and the main parameters of the elements are listed in table I for C^{6+} and U^{9+} ions in SSC1 and SSC2.

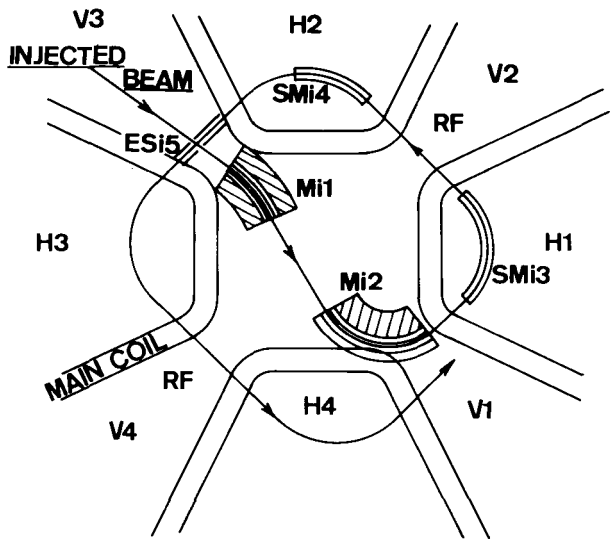

Fig. 2 Injection scheme

Models of M_{i2} and MS_{i3} will be built next year. The beam envelope along the injection path is quite smooth ; it is represented on Fig. 3.

The beam emittance for all ions is supposed to be :

ϵ_x = 45 mm.mrd at the entrance of SSC1
ϵ_z = 135 mm.mrd at the entrance of SSC1
ϵ_x = 11,25 mm.mrd at the entrance of SSC2
ϵ_z = 33,75 mm.mrd at the entrance of SSC2

Proc. 7th Int. Conf. on Cyclotrons and their Applications (Birkhäuser, Basel, 1975), p. 260-263

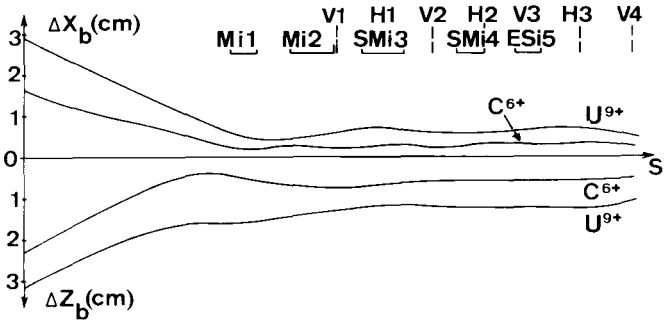

Fig. 3 Half beam size in SSC1 and SSC2 during injection

3. Ejection

Fig. 4 shows the azimuthal location of the extraction elements which are very similar to the injection ones.

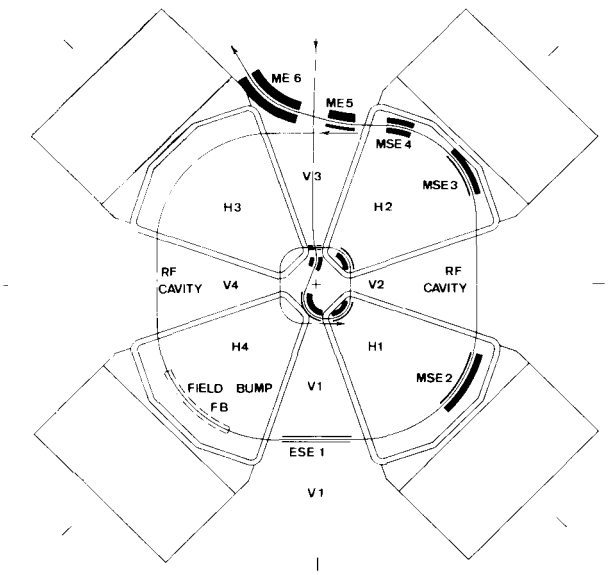

FIG4 - EJECTION SCHEME

A field bump coil giving a negative field $\Delta B(x, \theta)$ has been added in H_4 to increase the turn spacing when needed, as well as a focusing lens in H_2 to improve the beam quality of the outgoing beam. Table II gives the main characteristics of the extraction elements.

For SSC1, the whole range of ions should be extracted without too much difficulties with RF voltages significantly smaller than 250 kV ($\sigma \sim 20$ mm, beam width $\sim$ 10 mm). The beam envelope is drawn on Fig. 5.

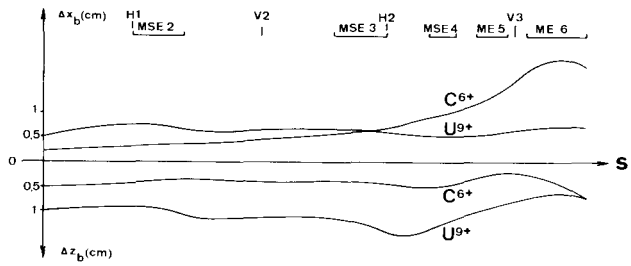

Fig. 5 Half beam size in SSC1 and SSC2 during ejection

In the case of SSC2, the natural turn spacing is not large enough as compared to the beam size ($\sigma \sim 2.5$ mm $\div$ 5 mm). The numerical computation has shown that it can be strongly increased by the means of a first harmonic negative field bump $\Delta B(x, \theta)$ even with a wave number $\nu_x \sim 1.2$ far from any resonant value. The radial dependance of $\Delta B(x)$ is represented on Fig. 6.

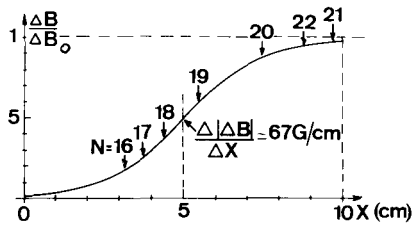

Fig. 6 Field bump $\Delta B(x)$; $\Delta B_0 = -333$ G

In order to make the beam behavior more clear, a first order study of the excitation process has been developped (3) (4) and is reported as follows.

The first order perturbed equation of motion, at the smooth approximation ($\beta_x \sim \frac{R}{\nu_x}$) is :

$$x''_\theta + \left[\nu_{x0}^2 - \left(\frac{R}{\rho}\right)^2 \Delta n(\theta)\right] x = \frac{R^2}{\rho} k\theta - R^2 \frac{\Delta B(\theta)}{(B\rho)} \quad (1)$$

where the three most important terms are selected.

$R = \frac{1}{2\pi} \times$ closed orbit length ~ 3 m

ρ = magnetic radius of curvature in sectors ~ 1.8 m

$R/\rho \sim 1.67$

$$\Delta n(\theta) = -\frac{\rho}{B} \frac{\Delta(\Delta B)}{\Delta x} \left[\Delta n_{max} = .75 \text{ for } B = 1.6\,T\right]$$

The linear term in θ provides the usual turn spacing σ_{RF} due to the RF acceleration. The ΔB term gives the closed orbit deformation which is increasing from turn to turn. A Fourier expansion of $\Delta B(\theta)$ limited to the first harmonic gives :

$$x = -\frac{R^2}{\rho}\frac{\varphi}{\pi}\left[\frac{1}{\nu_x^2} + \frac{2}{\nu_x^2 - 1}\cos\left(\theta + \frac{\pi}{4}\right)\right]\frac{\Delta B}{B} + \sigma_{RF}\frac{\theta}{2\pi} + A\cos\nu_x\theta + B\sin\nu_x\theta \qquad (2)$$

2φ = angular spread of $\Delta B(\theta) \sim 25°$

θ = 0 in the middle of V_1 (Fig. 4)

ΔB_{max} = - 330 G (Fig. 6)

If ΔB is small, particles follow the expanding equilibrium orbit with A = B $\sim$ 0. When ΔB comes near the maximum gradient, the variation in the closed orbit amplitude is so large that a betatron oscillation is induced (A , B $\neq$ 0). This can be observed on Fig. 7.

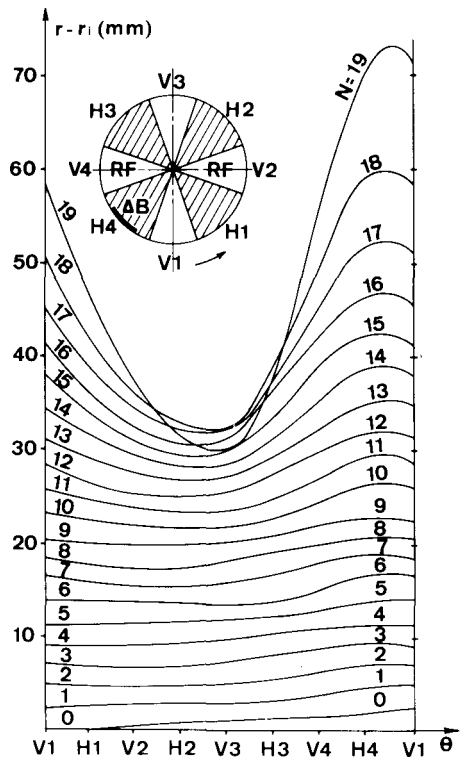

Fig. 7 Computed central orbit shape as a function of turn number N

The ν_x value in (2), decreasing with N (Δn effect in (1)) is easily obtained from a matrix calculation in the hard-edge approximation (Fig. 8) :

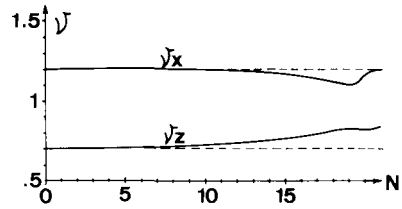

Fig. 8 ν values as a function of turn number N

$\nu_x \geq 1.1$, $\nu_z \leq .83$. It is also interesting to solve equation (1) with RHS equals zero around $2\nu_x = 2$ after having Fourier expanded $\Delta n(\theta)$. The ν_x stop band width so obtained gives an upper limit of the maximum gradient to be used as FB :

$$\Delta n < \frac{\pi}{2\varphi}\frac{\nu_{x_o}^2 - 1}{(R/\rho)^2} \sim 1.16 \qquad (3)$$

The total turn spacing σ at ES_{e1} azimuth (θ = 0), taking into account the full Fourier expansion of ΔB and neglecting the induced betatron oscillation is :

$$\sigma = \sigma_{RF}\left[1 - \frac{1}{\nu_x^2}\frac{R}{\rho}\cdot\frac{\sin\nu_x\varphi}{\sin\pi\nu_x}\cdot\cos\frac{3\pi}{4}\nu_x\cdot\frac{R}{B}\frac{|\Delta B|}{\Delta x}\right]^{-1} \qquad (4)$$

$\sim 2.5\ \sigma_{RF}$ with $\nu_x = 1.2$ and Δn_{max}

$\longrightarrow \infty$ with $\nu_x = 1.11$ (cf Fig. 8)

with $\sigma_{RF} \sim \frac{R}{2\nu_x^2}\frac{\Delta W_{turn}}{W}$

In fact, the increase in σ with decreasing ν_x is not so fast as predicted by (4) : let us recall that a first order treatment has been used.

It is however sufficient to provide ejection with well separated turns ($\sigma \sim$ 15 mm $>$ beam width $\sim$ 5 mm) as shown on Fig. 9. No significant effect is observed on the axial phase space trajectories during this process ($\nu_z \nearrow$, $\beta_z \searrow$).

The RF phase slip $\Delta\phi_{RF}$ is due to the first term in (2) :

$$\Delta\phi_{RF} \sim -2\pi h\frac{R}{\rho}\frac{\varphi}{\pi}\frac{1}{\nu_x^2}\int_0^N\frac{\Delta B}{B}dN \sim 2°3 \qquad (5)$$

h = SSC2 RF harmonic number = 2

ν_x = 1.1

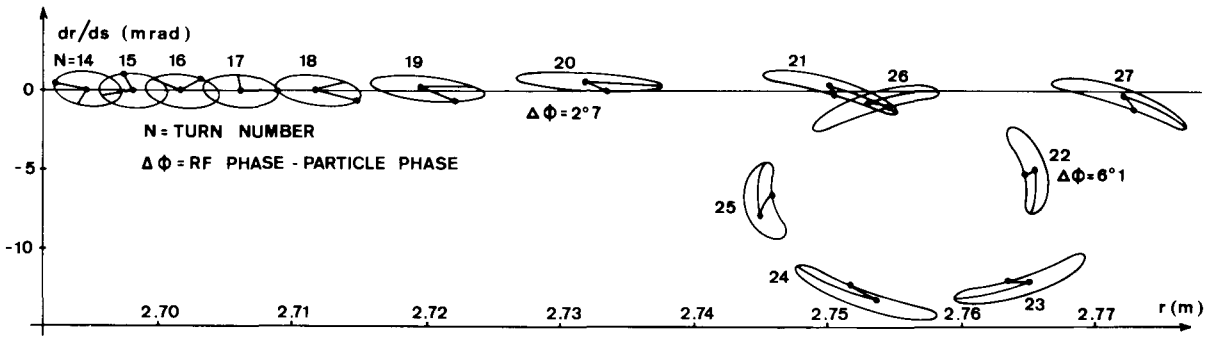

Fig. 9 Radial phase space trajectories and RF phase slip with a field bump FB

As a conclusion, the non resonant ($\nu_x = 1.2$) ejection process with a moderate linear field bump $\Delta B(x)$ is consistant with first order studies. With a well separated beam at the septum level, the extraction efficiency should be very high.

References

(1) GANIL group : "Avant projet de l'Accélérateur National d'Ions Lourds", April 1975.

(2) J. Fermé : "Description des programmes TRAJ 22 et TRAJ 30", Internal report, May 1975.

(3) J. Fermé, G. Gendreau, P. Yvon : "Etude analytique de l'extraction du faisceau par défaut de champ d'harmonique 1 - Partie 1", Internal report GANIL 75-14, June 1975.

(4) J. Fermé, G. Gendreau, P. Yvon : "Comportement du faisceau à l extraction au voisinage des résonances $p\nu_x = p$ - Partie 2", Internal report GANIL 75-19 July 1975.

TABLE I - Injection elements

	SSC1 : U^{9+}, $W_i = \frac{9.1}{(16)^2}$ MeV/A					SSC2 : C^{6+}, $W_i = \frac{93}{16}$ MeV/A				
Element	M_{i1}	M_{i2}	MS_{i3}	MS_{i4}	ES_{i5}	M_{i1}	M_{i2}	MS_{i3}	MS_{i4}	ES_{i5}
Max.field (T, kV/cm)	-1.1	1.9	.3	.11	2	-1.2	1.87	.28	.1	28
Curvature angle (°)	34	104	79	46	4	34	106	79	46	4
Face angle (°)	14	10	10	0	0	20	15	10	0	0
Gap (cm)	4	3	3	3	3	4	3	3	3	3
Useful aperture (cm)	4	3	3	3	3	4	3	3	3	3

TABLE II - Ejection elements

	SSC1 : U^{9+}, $W_e = \frac{9,1}{16}$ MeV/A							SSC2 : C^{6+}, W_e = 93 MeV/A						
Element	FB	ES_{e1}	MS_{e2}	MS_{e3}	MS_{e4}	M_{e5}	M_{e6}	FB	ES_{e1}	MS_{e2}	MS_{e3}	MS_{e4}	M_{e5}	M_{e6}
Max.field (T, kV/cm)	-.033	5	-.04	-.17	-.06	1	2	-.033	60	-.1	-.2	0	1	2
Curvature angle (°)		0	30	30	15	12	45		0	30	30	15	12	45
Max.gradient (T/m)	-.67	0	0	1.3	2	0	0	-.67	0	0	1.3	2	0	0
Gap (cm)	5	2	2.5	2.5	3	2	2	5	2	2.5	2.5	3	2	2
Useful aperture (cm)		7	3	3	5	10	10		7	3	3	5	10	10